A Friction-Based Kinematic Model for Skid-Steer Wheeled Mobile Robots

Sadegh Rabiee[1] and Joydeep Biswas[1]

***Abstract*— Skid-steer drive systems are widely used in mobile robot platforms. Such systems are subject to significant slippage and skidding during normal operation due to their nature. The ability to predict and compensate for such slippages in the forward kinematics of these types of robots is of great importance and provides the means for accurate control and safe navigation. In this work, we propose a new kinematic model capable of slip prediction for skid-steer wheeled mobile robots (SSWMRs). The proposed model outperforms the state-of-the-art in terms of both translational and rotational prediction error on a dataset composed of more than $6km$ worth of trajectories traversed by a skid-steer robot. We also publicly release our dataset to serve as a benchmark for system identification and model learning research for SSWMRs.**

I. INTRODUCTION

Skid-steer is a type of drive system, in which the wheels or tracks on each side of the vehicle are driven independently and turning is realized by means of driving the left and right wheels at different velocities. Such drive systems are popular due to their simplicity (no explicit turning mechanism) and maneuverability as they can turn in very small radii of curvature.

The disadvantage of skid-steer mobile robots (SSMR), on the other hand, is that slippage and skidding are inherent to these types of robots, which in turn makes it challenging to predict their motion accurately. In order to overcome this problem, various kinematic and dynamic models have been developed for this family of robots [1], [2], [3]. Historically, the kinematic models have proven more popular due to their simplicity and their robustness to inaccurate parameter estimates. The available kinematic models for SSWMRs and in general SSMRs either do not reason about slip [3] or if they do, it is by means of empirical relations that cannot be interpreted physically and hence are not generalizable to different platforms [4], [5]. In this work, we propose the friction-based kinematic model, which is a physically interpretable model that is capable of predicting the robot's slippage through reasoning about the wheel-ground interaction model. We also introduce and publicly release a comprehensive dataset for system identification research on SSWMRs which consists of more than $6km$ worth of trajectories traversed by a Clearpath Jackal robot on three different types of terrain. In summary, our contributions are as follows:

- A physically interpretable kinematic model for SSWMRs that predicts slippage due to the dynamics.
- A benchmark dataset of more than $6km$ worth of trajectories, well-suited for studying the kinematics and dynamics of SSWMRs.
- A survey and comparison of previous work on kinematic models for skid-steer mobile robots.

Our results show that the friction-based kinematic model can successfully capture the dynamics of the robot to predict slippage, and hence provides more accurate predictions of the robot's motion when compared to the state-of-the-art on a real-world dataset.

[1]Sadegh Rabiee and Joydeep Biswas are with the College of Information and Computer Sciences, University of Massachusetts Amherst, Amherst, MA, USA. Email: {srabiee, joydeepb}@cs.umass.edu

II. BACKGROUND AND RELATED WORK

Extended differential drive [3] is the most common and the simplest kinematic model for SSMRs. It based on the model used for differential drive systems. In this model the relation between the wheel velocities and the robot velocity is expressed as

$$\begin{bmatrix} v_x \\ v_y \\ v_\phi \end{bmatrix} = \frac{r}{B\chi} \begin{bmatrix} \frac{B\chi}{2} & \frac{B\chi}{2} \\ 0 & 0 \\ -1 & 1 \end{bmatrix} \begin{bmatrix} \omega_l \\ \omega_r \end{bmatrix}, \tag{1}$$

where ω_l and ω_r represent the angular velocity of the left and right wheels, respectively. v_x, v_y and v_ϕ denote the longitudinal, lateral, and angular velocities of the robot, respectively. r is the effective wheel radius and B is the track width of the robot as shown in Fig. 1. χ is a terrain-dependent parameter, called the ICR coefficient, where ICR is the instantaneous center of rotation. χ has values in the range $[1,\infty)$, where $\chi = 1$ corresponds to the case when there is no slippage and the kinematic model would be equivalent to that of an ideal differential drive system.

While the extended differential drive model assumes zero lateral velocity for the robot, i.e. $v_y = 0$, and also considers the robot to be symmetric, a **full linear model** [6] does not neglect the terms related to v_y and it allows for asymmetries as well. This model is described as

$$\begin{bmatrix} v_x \\ v_y \\ v_\phi \end{bmatrix} = A \begin{bmatrix} \omega_l \\ \omega_r \end{bmatrix}, \tag{2}$$

where A is a 3×2 matrix. Compared to the extended differential drive model, this model has 4 more parameters to be trained for. The idea behind this method of modeling SSWMR kinematics is to capture some of the nonlinearities of the system caused by slippage as well as asymmetries, such as different tire pressures, by means of a general linear model. Both the full linear and the extended differential drive models are trained using linear regression methods.

A class of SSMR kinematic models are mainly based on the radius of curvature of the robot's motion. These **ROC-based kinematic models** are derived experimentally and try to model the observation that SSMRs turn at relatively lower rates at small radii of curvature. Moosavian et al. [4] propose an exponential relation between the amount of slippage and the radius of curvature based on the experiments that they conduct on a skid-steer tracked robot. Wang et al. [5] also experiment on a SSWMR and deduce the relation between the ICR coefficient χ and radius of curvature to be of the form

$$\chi = 1 + \frac{b_1}{1 + b_2 |R_{ICR}|^{0.5}}, \tag{3}$$

where R_{ICR} denotes the radius of curvature. b_1 and b_2 are positive constant values that are terrain-dependent and are learned by observing the behavior of the robot while performing turning maneuvers at different radii of curvature.

At the wheel level, slip ratio s and slip angle α are defined as

$$s = 1 - \frac{V_{w_x}}{r\omega} \quad \text{and} \quad \alpha = \arctan(\frac{V_{w_y}}{V_{w_x}}), \tag{4}$$

where V_{w_x} and V_{w_y} are the longitudinal and lateral velocities of the wheel center, respectively. r denotes the wheel radius and ω is the wheel angular velocity. The relation between slip values and contact forces are extensively studied in the field of terramechanics and in the form of wheel-ground contact models [7], [8], [9]. For instance, a piecewise linear model states that the slip ratio s and slip angle α are linearly proportional to the normalized longitudinal and lateral friction forces applied to the wheel up to a limit. Seegmiller et al. [10] extend such linear wheel-level force-slip relation to the body level and propose an **enhanced kinematic model** that predicts slip. In their approach, robot's velocity is first predicted assuming zero slip, i.e. similar to (1) while $\chi = 1$, and then a residual linear and angular velocity is calculated and added to the original predicted values:

$$\vec{v}_{lin,slip} = (p_1 \frac{f_{lon}}{N} v_x + p_2 v_x)\hat{x} + (p_3 \frac{f_{lat}}{N} v_x)\hat{y}$$
$$v_{\phi,slip} = p_4 \frac{f_{lat}}{N} v_x + p_5 v_x + p_6 v_\phi,$$

where $\vec{v}_{lin,slip}$ and $v_{\phi,slip}$ are the residual values or body-level linear and angular slip velocities, respectively. f_{lon} and f_{lat} denote the longitudinal and lateral forces applied to the center of gravity and consist of the centrifugal and gravitational forces and N is the normal force. $p_{1:6}$ are constants and the parameters of the model. For more details on the meaning behind each of the parameters, please refer to [10]. Our work is similar to Seegmiller's enhanced kinematic model in that it builds upon the wheel-ground contact models to predict slip; however, its advantage is twofold: first, it is physically interpretable and based on the wheel-ground interaction model at the wheel level, while the enhanced kinematic model uses such friction models at the body level and with no physical proof. Second, our approach is capable of predicting slippage caused due to the dynamics of the robot, while the enhanced kinematic model assumes constant velocity motion. In the next section, we will explain our proposed method in detail.

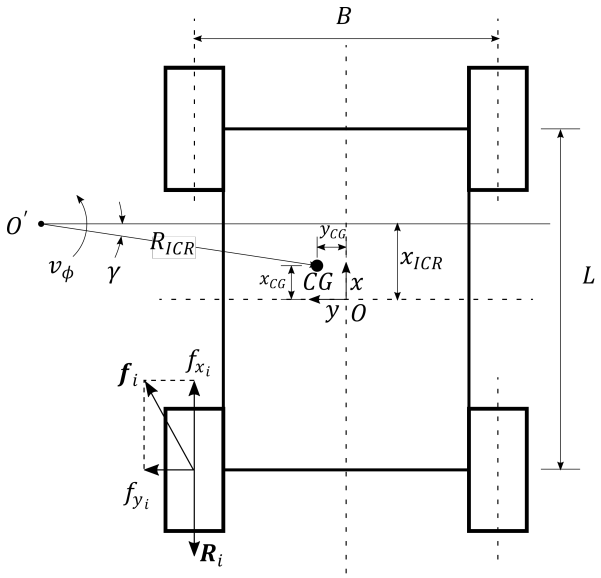

Fig. 1: Diagram of a skid-steer mobile robot performing a turning maneuver.

III. FRICTION-BASED KINEMATIC MODEL

A kinematic model provides an estimate of the robot's velocity given the pose and velocity of its joints, e.g. wheel velocities in the case of a wheeled mobile robot. We introduce the friction-based kinematic model, an extended kinematic model for SSWMRs that is capable of predicting slip caused by the dynamics of the robot. This model requires only one more input aside from the wheel velocities and that is the wheel acceleration. The proposed approach leverages the underlying knowledge of the wheel-ground contact model to predict wheel slippage given only the commanded wheel velocities and their derivatives.

Fig. 1 depicts a diagram of a skid steer robot performing a turn and illustrates the tractive and resistance forces applied to the robot. The point O' on the diagram depicts the instantaneous center of rotation of the robot (ICR) and x_{ICR} is the longitudinal offset of the ICR from the geometrical center of the robot. The local reference frame of the robot is defined on its geometric center O, and the robot's center of gravity is denoted by CG. The illustrated forces that are applied to the i^{th} wheel include the rolling resistance force $\mathbf{R}_i$ and the tractive force $\mathbf{f}_i$. $\mathbf{R}_i$ models the loss of energy caused by the non-elastic deformations of the tire and the ground and is exerted in the opposite direction of movement along the longitudinal axis and is written as

$$\mathbf{R}_i = \mu_r N_i, \tag{5}$$

where μ_r is the coefficient of rolling resistance and N_i is the normal force at the i^{th} wheel. The tractive force $\mathbf{f}_i$ is exerted in the opposite direction of the slip and has the components f_{x_i} and f_{y_i} that are related to the slip ratio s and slip angle α given the wheel-ground contact model. In this work we use a piecewise linear model and an exponential model for the

longitudinal and lateral contact forces, respectively [11].

$$f_x = \text{sgn}(s)\,\text{sgn}(V_{w_x})\min(|s|\lambda N, \mu_x N) \quad \text{and} \tag{6}$$

$$f_y = -\,\text{sgn}(V_{w_y})\mu_y(1-e^{-|\alpha|/C})N\,, \tag{7}$$

where f_x and f_y denote the tractive forces along the longitudinal and lateral axes, respectively. N is the normal force at the contact point, μ_x and μ_y are the coefficients of friction along the longitudinal and lateral axes, and λ and C are constant positive scalar parameters of the above friction models.

Given the commanded wheel velocities $\mathbf{u}_t = [\omega_{l_t}, \omega_{r_t}]^T$ and their derivatives $\dot{\mathbf{u}}_t = [\dot{\omega}_{l_t}, \dot{\omega}_{r_t}]^T$, we want to estimate the actual velocity of the robot in its local reference frame at time t denoted by $\mathbf{V}_t = [v_{x_t}, v_{y_t}, v_{\phi_t}]^T$. First, we will show the relation between $\mathbf{V}_t$ and $\mathbf{u}_t$ assuming we have the left and right wheel slip ratios s_{l_t}, s_{r_t} as well as the ICR longitudinal offset x_{ICR_t} for time t. Then we will explain how we can estimate the slip ratios and the ICR offset by means of estimating the forces applied to the robot at time t given only the commanded velocities $\mathbf{u}_t$ and their derivative $\dot{\mathbf{u}}_t$.

We add the notion of wheel slippage, as defined in (4), to the differential drive kinematic model, i.e. (1) with $\chi = 1$, and also take into account the effect of a non-zero ICR offset x_{ICR}. Hence, the relation between the wheel velocities and the robot velocity in the local reference frame is written as

$$\begin{bmatrix} v_{x_t} \\ v_{y_t} \\ v_{\phi_t} \end{bmatrix} = \frac{r}{B} \begin{bmatrix} \frac{(1-s_{l_t})B}{2} & \frac{(1-s_{r_t})B}{2} \\ x_{ICR_t}(1-s_{l_t}) & -x_{ICR_t}(1-s_{r_t}) \\ -(1-s_{l_t}) & (1-s_{r_t}) \end{bmatrix} \begin{bmatrix} \omega_{l_t} \\ \omega_{r_t} \end{bmatrix}. \tag{8}$$

Let $\theta_t = \{s_{l_t}, s_{r_t}, x_{ICR_t}\}$ denote the slip values and the ICR offset for time t. If we estimate θ_t, we can then plug it into (8) to calculate the robot velocity given the wheel velocities. Writing the dynamic equations of motion of a rigid body for our robot yields a nonlinear system of equations $\mathbf{F}(\theta_t)$

$$F_1(\theta_t) = \sum_{i=1}^{i=4} f_{x_i} - \sum_{i=0}^{i=3} \mathbf{R}_i - Ma_x \tag{9}$$

$$F_2(\theta_t) = \sum_{i=1}^{i=4} f_{y_i} - Ma_y \tag{10}$$

$$F_3(\theta_t) = \sum_{i=1}^{i=4} \tau_{\mathbf{f}_i} + \sum_{i=1}^{i=4} \tau_{\mathbf{R}_i} - I_z a_\phi\,, \tag{11}$$

where M is the mass of the robot, and I_z is its moment of inertia around the CG. $\tau_{\mathbf{f}_i}$ and $\tau_{\mathbf{R}_i}$ denote, respectively, the applied torque to the robot around the CG by the tractive force $\mathbf{f}_i = f_{x_i}\hat{x} + f_{y_i}\hat{y}$ and the rolling resistance force $\mathbf{R}_i$ at the i^{th} wheel. a_x and a_y are the linear acceleration of the CG along the x and y axes of the local reference frame respectively, and a_ϕ is the angular acceleration of the robot.

We will now walk through the steps to write the system of equations $\mathbf{F}(\theta_t)$ in terms of the unknown variables $\theta_t = \{s_{l_t}, s_{r_t}, x_{ICR_t}\}$ and the inputs $\mathbf{u}_t$ and $\dot{\mathbf{u}}_t$. First, we write a_x and a_y in terms of the velocity of CG, $\mathbf{v_{CG}} = v_{CG_x}\hat{x} + v_{CG_y}\hat{y}$, and its derivative, $\dot{\mathbf{v}}_{\mathbf{CG}}$.

$$a_x = \dot{v}_{CG_x} + \frac{||\mathbf{v_{CG}}||^2 \sin(\gamma)}{R_{ICR}}$$

$$a_y = \dot{v}_{CG_y} + \frac{||\mathbf{v_{CG}}||^2 \cos(\gamma)}{R_{ICR}}\,,$$

where γ (see Fig. 1), and v_{CG} are written in terms of $[v_{x_t}, v_{y_t}, v_{\phi_t}]^T$, which in turn are written in terms of θ_t and $\mathbf{u}_t$ as shown in (8):

$$v_{CG_x} = v_x - y_{CG} v_\phi$$

$$v_{CG_y} = v_y + x_{CG} v_\phi$$

$$\gamma = \arctan\left(\frac{(x_{ICR} - x_{CG})v_\phi}{v_x}\right).$$

Next, $\dot{v}_{CG_x}$, $\dot{v}_{CG_y}$, and a_ϕ are substituted with the commanded acceleration values $\dot{v}_{cmd_x}$, $\dot{v}_{cmd_y}$, and $\dot{v}_{cmd_\phi}$, defined as

$$\dot{v}_{cmd_x} = (\dot{\omega}_{r_t} + \dot{\omega}_{l_t})r/2$$

$$\dot{v}_{cmd_y} = 0$$

$$\dot{v}_{cmd_\phi} = (\dot{\omega}_{r_t} - \dot{\omega}_{l_t})r/B$$

where $\dot{\omega}_{r_t}$ and $\dot{\omega}_{l_t}$ are the rate of change of the commanded velocities to the right and left wheels, respectively.

It should be noted that replacing the actual acceleration values with the corresponding commanded values is a simplifying assumption that allows us to reach a rough estimate of the slippage caused by the dynamics of the robot. While in reality the robot might not reach the commanded acceleration due to slippage and the motor dynamics, this simplifying assumption could be thought of as a zero-order approximation of the robot acceleration. It should also be noted that we are assuming the commanded velocities to comply with the acceleration limits of the robot, which is a reasonable assumption as motion planners often take into account the hardware limits of the robot.

As a result, a_x, a_y, and a_ϕ are written in terms of θ_t, $\mathbf{u}_t$, and $\dot{\mathbf{u}}_t$. f_{x_i} and f_{y_i} are also written in terms of θ_t and $\mathbf{u}_t$ via (6) and (7). Thus, (9), (10), and (11) can be written in terms of θ_t, $\mathbf{u}_t$, and $\dot{\mathbf{u}}_t$. At each time step t, we have $\mathbf{u}_t$ and $\dot{\mathbf{u}}_t$ as inputs and we solve the nonlinear system of equations $\mathbf{F}(\theta) = 0$ for θ via trust-region optimization such that

$$\theta = \underset{\theta'}{\text{argmin}}\, F(\theta')^T F(\theta')\,. \tag{12}$$

Then we plug θ into (8) which in turn yields the predicted velocity of the robot $\mathbf{V}_t$.

The parameters of the friction-based kinematic model , i.e. $\{\mu_r, \mu_x, \mu_y, \lambda, C\}$ are trained through nonlinear least squares optimization such that the error in predicted velocity of the robot is minimized over the training dataset.

The friction-based kinematic model lies at the region between kinematic models and dynamic models. It is similar to dynamic models in that it reasons about the forces applied to the robot; however, it does not use the estimated forces to calculate and integrate over the acceleration values. Instead, it only uses the estimated forces to predict slip given the wheel-ground interaction models. We classify our method as a kinematic model because of its inputs and outputs at the

TABLE I: DATASET STATISTICS

Category	Terrain Type	Name	Duration (s)	Traversed Distance (m)	Absolute Rotation (deg) $\times 10^3$	Lin. Vel. Mean (m/s)	Lin. Vel. Std. (m/s)	Ang. Vel. Mean (deg/s)	Ang. Vel. Std. (deg/s)	Wheel Slip Vel. Mean (m/s)	Wheel Slip Vel. Std. (m/s)
Training	Tile	Train1	384	463.2	31.1	1.30	0.48	34.3	48.6	0.15	0.12
	Asphalt	Train2	355	417.9	24.1	1.31	0.44	32.7	40.1	0.18	0.12
	Grass	Train3	977	764.1	64.8	0.87	0.25	33.3	38.9	0.13	0.06
Constant Velocity	Tile	CV1	2059	910.3	117.6	0.48	0.48	29.8	29.2	0.11	0.10
	Asphalt	CV2	1083	459.4	72.0	0.47	0.45	31.5	17.2	0.12	0.08
	Grass	CV3	2127	771.1	133.8	0.40	0.41	31.19	24.9	0.12	0.08
Long Distance	Tile	LD1	978	686.0	22.5	0.84	0.61	8.0	14.0	0.08	0.10
	Asphalt	LD2	906	1070.8	17.9	1.33	0.48	9.7	14.4	0.07	0.08
	Grass	LD3	685	561.5	13.2	0.88	0.26	12.8	16.5	0.08	0.05

high level regardless of the underlying reasoning about the dynamics of the robot.

IV. DATASET

Data Collection Setup. We use the Clearpath Jackal, which is a $16kg$ mobile robot with a skid-steer drive system used mainly as a research platform. The Jackal has a top speed of $2m/s$ and has two motors, each of which controls the two wheels on each side of the robot. For all experiments, the tire pressure is adjusted to the nominal value of $20psi$. A pair of Point Grey Blackfly cameras are used for localization using stereo visual odometry at $30Hz$. Fig. 2 shows the experiment platform setup. During the experiments, the robot is driven and the camera feed, commanded velocities ($45Hz$), IMU readings ($75Hz$), and wheel odometry ($20Hz$) are logged. The logged data is then used for generating the ground truth trajectory traversed by the robot offline and using ORB-SLAM [12]. For all datasets, the above mentioned logged data as well as the ground truth are provided. The data is collected in different datasets based on the velocity and acceleration profile of the trajectories. In the following , we describe each of these categories and provide their statistics, which are summarized in Table I. The dataset is available at `https://amrl.cs.umass.edu/dataset/skid_steer`.

Training Dataset. The training dataset consists of sessions of the robot being driven using a joystick on three different surface types. The training dataset has a large diversity in the trajectories traversed by the robot in terms of both velocity and acceleration, i.e. it includes both trajectories of the robot performing wide turns at low velocities as well as instances of the robot being driven in sharp turns aggressively and with high acceleration.

Constant Velocity Dataset. This dataset consists of segments of the robot executing constant velocity turning trajectories in open loop on tile, asphalt, and grass surfaces. In each segment the robot is commanded a constant linear and angular velocity and this is repeated for different turning radii. The purpose of this dataset is to analyze the kinematics of the robot and the slippage while there are no dynamics involved.

Long Distance Traversal Dataset. The long distance traversal dataset consists of three uninterrupted sessions of the robot traversing a long path on tile, asphalt, and grass. This dataset includes more than $2.3km$ traversed by the robot in total. The purpose of this dataset is to have a benchmark for normal operation of the robot in real-world scenarios. For this dataset the robot is driven by a human operator using a joystick.

V. EXPERIMENTAL RESULTS

We implemented the friction-based kinematic model as well as the kinematic models discussed in section II, including the extended differential drive, the full linear model, the ROC-based model [5], and the enhanced kinematic model. Different instances of each model were trained for different types of terrain. We then tested the trained models on the constant velocity and long distance datasets with the same type of terrain. The models are evaluated based on their ability to predict the pose of the robot over a horizon h. At each time step t, given the current state of the robot $\mathbf{x}_t = [x_t, y_t, \phi_t]$, the sequence of future wheel velocity commands $\mathbf{u}_{t:t+h}$, and future wheel acceleration commands $\dot{\mathbf{u}}_{t:t+h}$, we calculate the predicted pose of the robot $\mathbf{x}_{t+h_{pred}}$ and the prediction error $err_t(h)$ for the prediction horizon h as

$$\mathbf{x}_{t+h_{pred}} = \mathbf{x}_t + \int_t^{t+h} f(\mathbf{x}_\tau, \mathbf{u}_\tau, \dot{\mathbf{u}}_\tau) d\tau$$
$$err_t(h) = \mathbf{x}_{t+h} - \mathbf{x}_{t+h_{pred}},$$

where $f(\mathbf{x}_\tau, \mathbf{u}_\tau, \dot{\mathbf{u}}_\tau)$ denotes the kinematic model of the robot that provides a prediction of its velocity $\dot{\mathbf{x}}_{\tau_{pred}}$ at time τ. $\mathbf{x}_{t+h}$

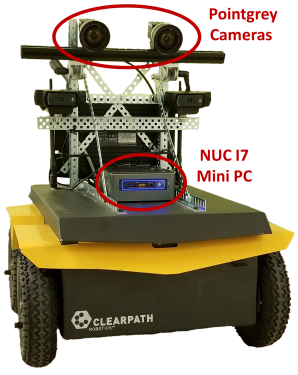

Fig. 2: Clearpath Jackal, the skid-steer platform used for the experiments.

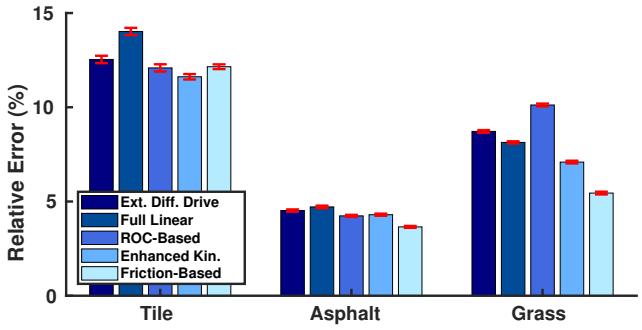

(a) Constant-Velocity dataset.

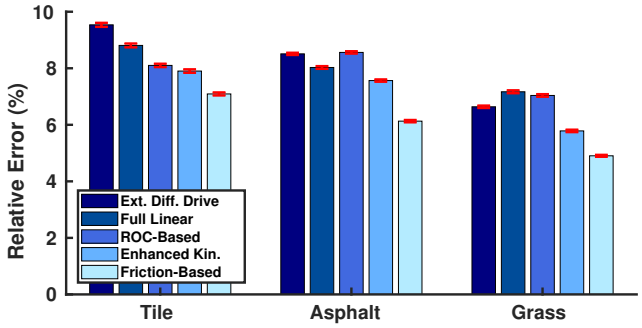

(b) Long-Distance-Traversal dataset.

Fig. 3: Translational prediction error for a 6-second prediction horizon for different kinematic models on different datasets.

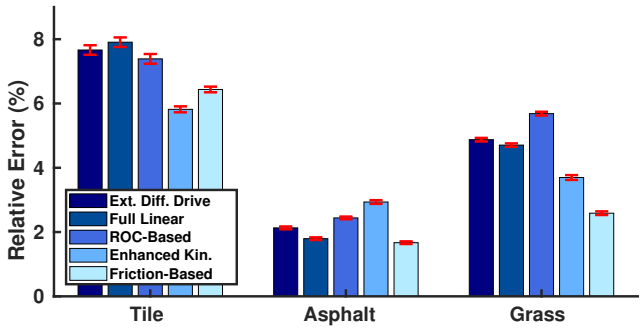

(a) Constant-Velocity dataset.

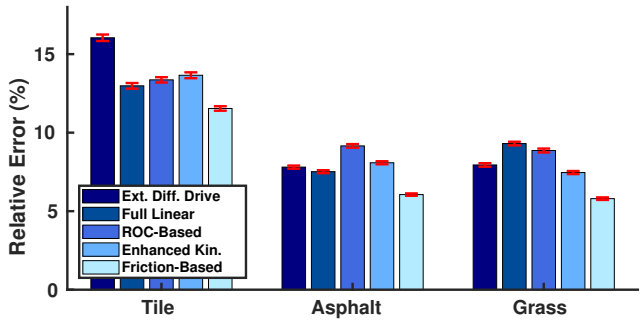

(b) Long-Distance-Traversal dataset.

Fig. 4: Rotational prediction error for a 6-second prediction horizon for different kinematic models on different datasets.

is the ground truth pose of the robot at time $t+h$ which is provided by stereo visual odometry.

Using visual odometry makes it possible to conduct experiments on long distance trajectories and on different types of terrain in a cost effective manner. Marker-based motion tracking systems [13] are only applicable to small scale experiments in lab settings. GPS provides localization only outdoors and with an accuracy of a couple of meters. RTK GPS systems [14] provide localization with accuracy of a few centimeters in the vicinity of a base station; however, such systems are very expensive and they do not provide any information about the orientation of the robot. In order to assure high accuracy localization, we run visual odometry offline and extract large numbers of image features. Through a set of experiments, we have measured the relative translational error of our localization setup to have a mean value of 0.4% and a standard deviation of 0.3%. We have also recorded a 0.2% mean and 0.2% standard deviation for the relative rotational error. During these experiments, the robot was driven starting at a marked point and returned back to the same point after more than $20s$ of driving. The difference of the initial and final pose of the robot estimated by the localization system was calculated as the localization error. Over 40 trials were recorded at the same locations as the actual dataset and the robot was driven at its full speed range.

Fig. 3a and 3b illustrate the root mean squared relative error (RMSRE) values of the translational prediction error of different kinematic models over a 6-second prediction horizon on the constant-velocity and long-distance-traversal datasets, respectively. Fig. 4a and 4b show the rotational prediction error for the same kinematic models and datasets. It should be noted that the figures show the relative error values that are normalized with respect to the robot's actual displacement and absolute rotation values over the prediction horizon. As it can be seen in the figures, the friction-based kinematic model performs significantly better than all other models in terms of both translational and rotational error on the long distance traversal dataset and it performs comparable to the other models on the constant velocity dataset. The result is expected since the friction-based kinematic model's advantage over other kinematic models stands out when the robot has accelerated motion, in which case the model's reasoning about the wheel-ground interaction model and the robot's dynamics allows it to capture nonlinearities in the motion model that the other kinematic models cannot.

In order to further investigate the motion model of the robot and the role of its dynamics in its behavior's deviation from a linear kinematic model, we have visualized the measured angular velocity of the robot given pairs of measured wheel velocities for the Test1 dataset in Fig. 5. The figure depicts a side view of the plane defined by the trained full linear kinematic model, $a_l\omega_l + a_r\omega_r = v_\phi$, that is overlaid with data points of observed angular velocities. The data points are colored based on the measured angular acceleration of the robot, such that the darker the color, the lower the angular acceleration. As it can be seen, the deviation of the observations from the values predicted by the linear model (the plane), is not random. The prediction error $\delta v_\phi = v_{\phi_{measured}} - v_{\phi_{pred}}$ and the acceleration value are negatively correlated, such that with increase in angular

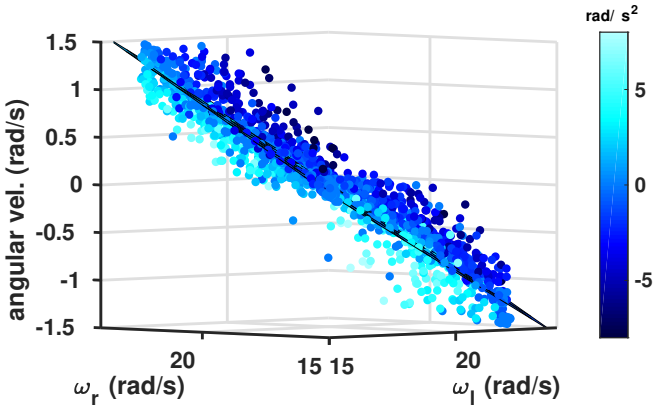

Fig. 5: Measured angular velocities of the robot for different wheel velocities and different angular acceleration values. Increase in angular acceleration leads to decrease in observed angular velocity for the same pair of wheel velocities

acceleration, the observed angular velocity decreases for the same pair of wheel velocities $\{\omega_l, \omega_r\}$. While this observation matches our intuition of the dynamics of the robot, it also signifies the fact that the dynamics of an SSWMR play a remarkable role in describing the motion of the robot, which is the motivation behind our proposed kinematic model. The friction-based kinematic model goes beyond the normal definition of a kinematic model and predicts the robot's slipping by means of taking the commanded acceleration values as an approximation of the robot's actual acceleration. Fig. 6 visualizes the predicted robot angular velocities by the friction-based kinematic model given the commanded wheel velocities at different commanded angular acceleration values. The three surfaces in the figure, represent the friction-based kinematic model's predictions of the robot's angular velocity for three different values of commanded angular acceleration $\dot{v}_{cmd_\phi} = \{-8rad/s^2, 0rad/s^2, 8rad/s^2\}$ and zero commanded linear acceleration. The surface moves toward negative angular velocity direction with increase in the commanded angular acceleration, which is in line with our observations of the robot's actual behavior as shown in Fig. 5.

Fig. 7 depicts multiple snapshots of actual robot trajectories from both constant velocity and long distance traversal datasets. The ground truth measurement as well as the predicted trajectories by different kinematic models are depicted for a 6-second prediction horizon. As it can be seen the friction-based kinematic model predicts the robot's slippage, and hence the actual trajectory, more accurately than other kinematic models. It is worth noting that having an accurate forward model that can predict the pose of the robot over a long horizon in the future is of paramount importance for safe navigation and motion planning and has applications in model predictive planning algorithms [15], where an accurate motion model would significantly improve the effectiveness of such approaches.

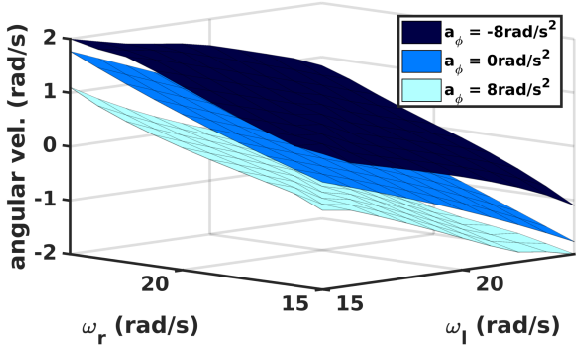

Fig. 6: Friction-based model's prediction of angular velocity for different wheel velocities and different angular acceleration values.

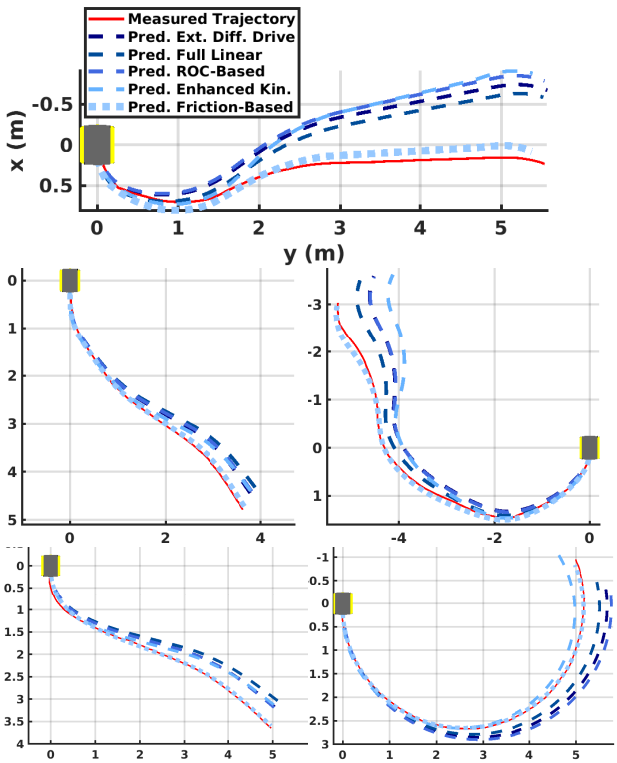

Fig. 7: Samples of actual robot trajectories and the predicted trajectories by different kinematic models for a 6-second prediction horizon.

VI. CONCLUSION

In this paper, we introduced the friction-based kinematic model for SSWMRs, which is physically interpretable and capable of predicting slippage caused by the dynamics of the robot. We compared our model against the state-of-the-art via testing on real-world data and it showed better performance in predicting both the position and orientation of the robot. We have also publicly released our dataset, consisting of more than $6km$ worth of trajectories traversed by an SSWMR on three different types of terrain. As future work, we would like to integrate the friction-based kinematic model into the controls of SSWMRs and develop a closed loop control system based on our kinematic model.

REFERENCES

[1] W. Yu, O. Chuy, E. G. Collins, and P. Hollis, "Dynamic modeling of a skid-steered wheeled vehicle with experimental verification," in *Intelligent Robots and Systems, 2009. IROS 2009. IEEE/RSJ International Conference on*. IEEE, 2009, pp. 4212–4219.

[2] K. Kozłowski and D. Pazderski, "Modeling and control of a 4-wheel skid-steering mobile robot," *International journal of applied mathematics and computer science*, vol. 14, pp. 477–496, 2004.

[3] A. Mandow, J. L. Martinez, J. Morales, J. L. Blanco, A. Garcia-Cerezo, and J. Gonzalez, "Experimental kinematics for wheeled skid-steer mobile robots," in *Intelligent Robots and Systems, 2007. IROS 2007. IEEE/RSJ International Conference on*. IEEE, 2007, pp. 1222–1227.

[4] S. A. A. Moosavian and A. Kalantari, "Experimental slip estimation for exact kinematics modeling and control of a tracked mobile robot," in *Intelligent Robots and Systems, 2008. IROS 2008. IEEE/RSJ International Conference on*. IEEE, 2008, pp. 95–100.

[5] T. Wang, Y. Wu, J. Liang, C. Han, J. Chen, and Q. Zhao, "Analysis and experimental kinematics of a skid-steering wheeled robot based on a laser scanner sensor," *Sensors*, vol. 15, no. 5, pp. 9681–9702, 2015.

[6] G. Anousaki and K. J. Kyriakopoulos, "A dead-reckoning scheme for skid-steered vehicles in outdoor environments," in *Robotics and Automation, 2004. Proceedings. ICRA'04. 2004 IEEE International Conference on*, vol. 1. IEEE, 2004, pp. 580–585.

[7] R. M. Brach and R. M. Brach, "Tire models for vehicle dynamic simulation and accident reconstruction," SAE Technical Paper, Tech. Rep., 2009.

[8] R. Brach and M. Brach, "The tire-force ellipse (friction ellipse) and tire characteristics," SAE Technical Paper, Tech. Rep., 2011.

[9] G. Ishigami, A. Miwa, K. Nagatani, and K. Yoshida, "Terramechanics-based model for steering maneuver of planetary exploration rovers on loose soil," *Journal of Field robotics*, vol. 24, no. 3, pp. 233–250, 2007.

[10] N. A. Seegmiller, "Dynamic model formulation and calibration for wheeled mobile robots," 2014.

[11] J. Wong and C. Chiang, "A general theory for skid steering of tracked vehicles on firm ground," *Proceedings of the Institution of Mechanical Engineers, Part D: Journal of Automobile Engineering*, vol. 215, no. 3, pp. 343–355, 2001.

[12] R. Mur-Artal and J. D. Tardós, "ORB-SLAM2: an open-source SLAM system for monocular, stereo and RGB-D cameras," *IEEE Transactions on Robotics*, vol. 33, no. 5, pp. 1255–1262, 2017.

[13] P. Merriaux, Y. Dupuis, R. Boutteau, P. Vasseur, and X. Savatier, "A study of vicon system positioning performance," *Sensors*, vol. 17, no. 7, p. 1591, 2017.

[14] R. B. Langley, "Rtk gps," *GPS World*, vol. 9, no. 9, pp. 70–76, 1998.

[15] G. Ishigami, K. Nagatani, and K. Yoshida, "Path planning and evaluation for planetary rovers based on dynamic mobility index," in *Intelligent Robots and Systems (IROS), 2011 IEEE/RSJ International Conference on*. IEEE, 2011, pp. 601–606.